STAFF SUMMARY SHEET

	TO	ACTION	SIGNATURE *(Surname)*, GRADE AND DATE		TO	ACTION	SIGNATURE *(Surname)*, GRADE AND DATE
1	DFAN	sig	Hall / LtCol / 19 Mar 13	6			
2	DFER	approve	Kerns, Col 19 Mar 13	7			
3	DFAN	action	(Author /Originator)	8			
4				9			
5				10			

SURNAME OF ACTION OFFICER AND GRADE McLaughlin, Civ	SYMBOL DFAN	PHONE 333-2613	TYPIST'S INITIALS tem	SUSPENSE DATE 20130320

SUBJECT Clearance for Material for Public Release USAFA-DF-PA- 227	DATE 20130319

SUMMARY

1. PURPOSE. To provide security and policy review on the document at Tab 1 prior to release to the public.

2. BACKGROUND.
Authors: C1C Ryan Petrie, Jurgen Seidel, Christopher Porter

Title: Computational Modeling of Shear Layer Distortions Over a Turret

Circle one: Abstract   Tech Report   Journal Article   Speech   (Paper)   Presentation   Poster
Thesis/Dissertation   Book   Other: _____

Check all that apply (For Communications Purposes):
[] CRADA (Cooperative Research and Development Agreement) exists
[X] Photo/ Video Opportunities   [] STEM-outreach Related   [] New Invention/ Discovery/ Patent

Description: The research presented in this paper concerns the computational simulation of the flow over an airborne turret that was performed incorporating computational fluid dynamics (CFD) with optical beam post processing.
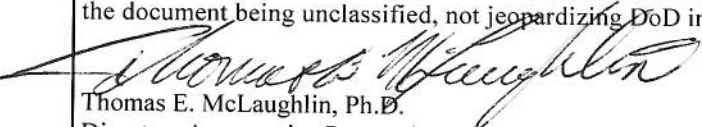
Release Information: To be presented at the AIAA Student Paper Competition, St Louis MO, 11-12 April 2013

Previous Clearance information: (If applicable): This work was internally funded. Similar papers regarding the AAOL turret have been published in the open literature.

Recommended Distribution Statement: Distribution A: approved for public release, distribution unlimited

3. DISCUSSION.

4. RECOMMENDATION. Sign coord block above indicating document is suitable for public release. Suitability is based solely on the document being unclassified, not jeopardizing DoD interests, and accurately portraying official policy.

Thomas E. McLaughlin, Ph.D.
Director, Aeronautics Research Center

Computational Modeling of Shear Layer Distortions Over a Turret

Ryan C. Petrie[*]

with

Dr. Jürgen Seidel[†] and Dr. Chris Porter[‡]

Department of Aeronautics, United States Air Force Academy, CO 80841

A current area of interest in the aeronautical community is the simulation of flow over an airborne turret. The research presented in this paper concerns the computational simulation of the flow over an airborne turret that was performed incorporating computational fluid dynamics (CFD) with optical beam post processing. The turbulence model used in the Cobalt CFD solver was the Delayed-Detached Eddy Simulation with Shear Stress Transport (DDES-SST) model. The CFD simulation matched flight conditions at an altitude of 15,000 feet and a Mach number of 0.4. The grid surrounding the turret contained 164M elements. After computing the flow field, the aero optical data reduction yielded the optical wave front distortions as the beam traversed the turret's wake. The ultimate goal is to use these modeling techniques to provide data to mitigate aberrations in the wave front resulting from the beam propagating through the flow field surrounding the airborne turret. The DDES-SST turbulence model provided an adequate model of a turret's wake for the given grid and aero-optic analysis techniques were used to determine the beam quality as it passes through the separated shear layer and the farfield irradiance.

Nomenclature

C_P	= coefficient of pressure	OPD_{RMS}	= root-mean-square of the OPD
I	= farfield irradiance	ρ	= density
I_0	= diffraction-limited farfield irradiance	Sr	= Strehl Ratio
K_{GD}	= Gladstone-Dale constant	θ	= position (from 0° to 180°) over turret's
λ	= wavelength		surface
n	= index of refraction	t	= time (seconds)
OPL	= Optical Path Length	Δt	= time step (seconds)
$\overline{OPL}$	= average Optical Path Length	$y^{'}$	= initial grid spacing in wall coordinates
OPD	= Optical Path Difference		

I. Introduction

USING high powered lasers mounted on airborne platforms has become an area of great interest in the last decade following early research in the 1950's. Advanced laser technology provides a means for both airborne directed energy applications as well as high-bandwidth line-of-sight communications. Such a laser would be emanated from a turret mounted somewhere on the aircraft's exterior. To maximize the effectiveness of airborne lasers, it is important to understand what influence the flow field around the turret has on the beam. More specifically, it is important to know how the wake behind the turret distorts and affects the beam's farfield irradiance through the nearfield density, and thus index of refraction, fluctuations around the turret. The nearfield in this case defines an optical region in which diffraction effects are negligible. It encompasses the area surrounding the turret where the turret's boundary layer and the shear layer behind the turret cause the most severe temperature and pressure changes. Once clear of this area, the beam traverses through the atmosphere until it reaches its target. In this case, the farfield is the undisturbed atmospheric region in which diffraction effects must be taken into account. The aero-optic analysis is only concerned with nearfield effects, as the atmospheric optics problem is addressed through other means. Understanding the nearfield problem is the goal of this computational fluid dynamics (CFD) investigation.

Computational fluid dynamics is an extremely useful tool in computing and visualizing the boundary layer on the turret as well as the wake behind it. These computational predictions can aid application developers in designing

---

an adaptive optic system to maximize the farfield irradiance. However, to date, CFD predictions of the flow around a turret have not reached a level of reliability necessary for design purposes.

In the current investigation, the Delayed-Detached Eddy Simulation – Shear Stress Transport (DDES-SST) turbulence model[1] was utilized within the Cobalt CFD solver to compute the flow over a turret with similar geometrical features as those on the Airborne Aero-Optics Laboratory (AAOL) turret shown in Fig. 1. Because turbulence models are designed to allow for the computation of flow fields that are not feasible with Direct Numerical Simulation (DNS) by modeling the effect of small flow scales onto the large, computed scales, the results often vary dramatically and their usefulness has been questioned. If it can be determined that the flow solution for the particular geometry and turbulence model captures flow structures that are expected for this type of flow field while accurately determining the separation point over the turret, the model can then be used in good faith to investigate the optical effects of the flow over a turret.

An example of two extremes from previous CFD simulations can be seen in Figs. 2 and 3. These computations were designed to attempt to mirror the behavior experienced by the turret on AAOL, however, the aperture used in the simulation was conformal (smooth, unlike what is seen in Fig. 1). Furthermore, there were no "smiles", which allow a full 180° rotation of the aperture, carved into the cylinder. The flow around the turret in Fig. 2 was computed with the DDES-Spalart-Allmaras turbulence model. The flow in Fig. 3 was computed using a laminar flow assumption (i.e. without a turbulence model).[2] Notable features of the flow visualization in Fig. 2 are the smooth shear layer coming off the top of the turret and large structures that form the wake. Essentially, the turbulence

Figure 1. AAOL optical turret.

model fails to correctly account for the small structures in the wake, showing premature dissipation and an unrealistic smoothness of the wake's structures. Figure 3, in contrast, shows a lot of small scale structures in the wake, but that does not necessarily indicate that the flow field is captured correctly. For instance, the necklace vortex which wraps around the front of the turret is much more complicated than in Fig. 2. In comparison, it is clear that with the turbulence model (Fig. 2), the horn vortices coming off the rear of the hemisphere of the turret are present, but minor structures in the shear layer and wake are removed by the turbulence model.
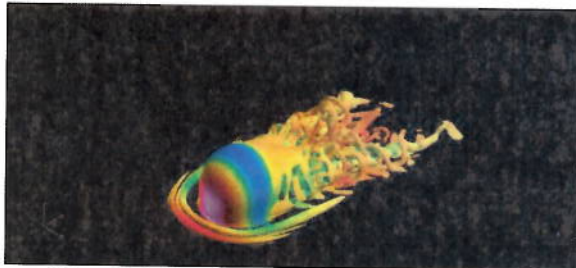

Figure 2. DDES-SA turbulence model flow visualization for a conformal turret.[2]
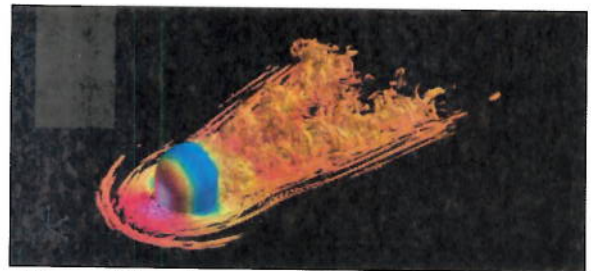

Figure 3. Laminar model flow visualization for a conformal turret.[2]

The centerline pressure distribution for these simulations were compared to experimental as well as theoretical data (Fig. 4). As expected, the data is in good agreement on the windward side of the turret. The computed separation point is slightly downstream of the experimentally measured location.
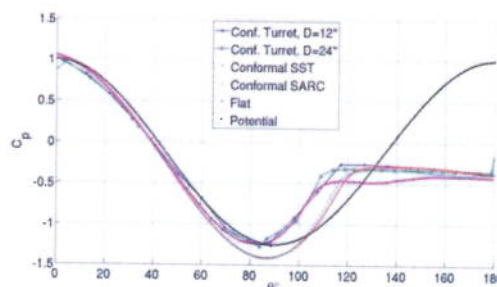

Figure 4. C_P as a function of θ for a series of previous experimental CFD simulations.[3]

In 2011, flight tests involving two Cessna jets used an airborne laser to measure aero optical effects of flow around a turret.[3] These experimental results form the foundation for the current simulations. For the first time in this field of research, aero optical distortions were experimentally quantified in flight for a flat- and conformal-windowed turret. The data was obtained using a Shack-Hartmann wave front sensor with a 31x31 lenslet array splitting up the optical aperture. For the optical analysis of the CFD data in Fig. 5, the resolution has been increased to simulate a 100x100 lenslet array.

A comparison of the optical data from the two simulations shown in Figs. 2 and 3 with this flight data is shown in Fig. 5. Normalized *OPD*, explained in detail later in this paper, is plotted against the azimuthal angle. From Fig. 5, it is clear that the laminar model over predicts the optical distortion in the wake of the turret, while the DDES-SST model under predicts the experimental data. However, it must be noted that the AAOL turret had a flat window aperture and smiles (see Fig. 1), while the CFD data was obtained with a conformal canonical turret.
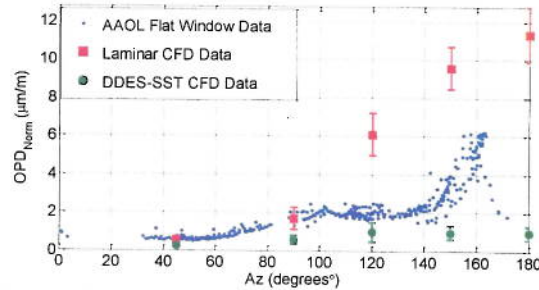

Figure 5. AAOL experimental data compared with CFD data.[3]

II. Setup and Procedures

A. Geometry Modeling

The turret geometry used in the computational simulations matches the basic shape and size of the turret used on the AAOL. This turret is designed with a flat aperture positioned at a 120° azimuth angle and a 50° elevation angle. Two "smiles" were cut into the cylindrical base to allow the beam to swivel 180° undisturbed; see Fig. 6. The turret is comprised of a 10 cm tall cylinder with a diameter of 30.5 cm and a hemisphere with a radius of 15.25 cm attached to the top of the cylinder. Carved into this hemisphere is the flat aperture with a diameter of 10.5 cm. The laser is designed to fire through the center of this aperture. The laser has a 10 cm diameter, which leaves a .25 cm thick ring around the laser on the aperture's surface. This ring will be used to house pressure transducers which will provide feedback on the current flow state and optical aberrations in the beam for eventual feedback control of both the flow and use of adaptive optics to improve performance.

The mesh is built in a rectangular domain 400 cm wide, 600 cm long, and 200 cm tall. Compared to similar wind tunnel research with a typical 1m x 1m x 3m test section, the domain used in the CFD experiment is nearly twenty times larger than the wind tunnel test section. The turret sits on the base of this domain in the center of the width and 200 cm from the inflow boundary. Figure 7 shows the computational domain. In this figure, air flows from the bottom left to the top right of the domain.
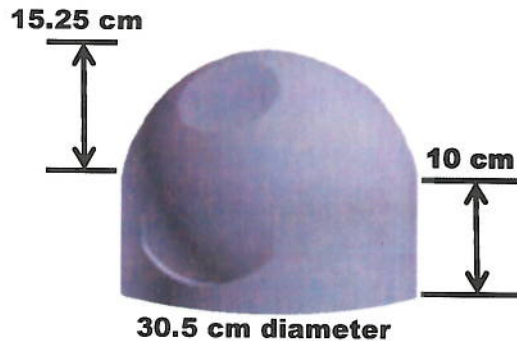

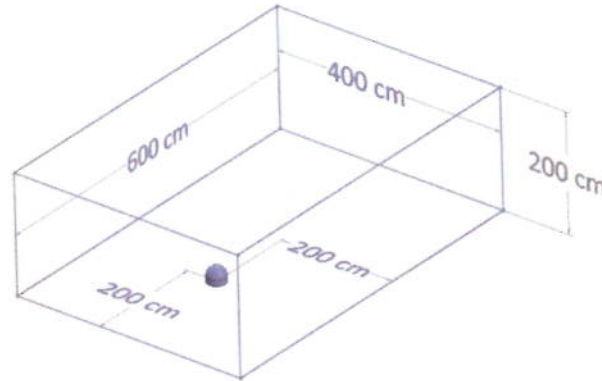Figure 6. Turret being used in this computational simulation.

3

Figure 7. Box used to contain mesh grid around turret.

The mesh used is comprised of a boundary layer grid on the floor and turret and an unstructured tetrahedral grid filling in the rest of the space. This allows the computational model to resolve the flow in the boundary layer while minimizing the computational overhead in areas of less interest. A two dimensional view of this mesh on the turret's centerline is shown in Fig. 8. The nodes are clustered near the surface of the turret where accurately resolving the flow is crucial. The specific initial y^+ value is about 0.03 with a steady 20% increase.

Figure 8. Two dimensional view of the hybrid mesh around the turret.

B. Computational Modeling

i. DDES-SST

It is crucial to properly resolve the flow near the surface of the turret and the aircraft (simulated as the domain's floor). The Delayed Eddy Simulation (DES) model developed by Spalart, which uses the Reynolds-Averaged Navier Stokes (RANS) model to capture the flow near the boundary of a grid, is used in the current simulations[1]. In DES, Large Eddy Simulation (LES) is used in places where computer resources allow and accuracy is needed. Spalart's hybrid model resolves the flow using the most accurate but time efficient model in a given region of the grid. However, a number of shortcomings of the DES model have been identified, which were corrected with the introduction of the Delayed-Detached Eddy Simulation (DDES) model. In this model, a blending function is used to transition between RANS and LES independent of grid spacing, making the transition more efficient and inclusive.[1]

The Shear Stress Transport (SST) model used in conjunction with DDES was developed by Menter.[4] The SST model combines the k-ω and k-ε models; one focuses on the inner boundary layer and the other focuses on the outer region and outside the boundary layer. The weakness of the k-ω model is that it is dependent upon freestream values in relation to the Reynolds number, which limits its accuracy near the wall. The weakness of the k-ε model is that it over-predicts the shear stress in regions of adverse pressure gradient. To improve on both of these models, Menter combined the two models and adjusted various constants to develop the SST model. This new model not only overcomes the disadvantages of the two separate models, but also proves to be very accurate in resolving flow over walls that introduce highly separated regions of flow.[4] With these characteristics, the DDES-SST model should be very well suited for computing the flow over a turret where large regions of highly separated flow are present.

ii. Simulation Parameters

The simulations were designed to compare to flight tests conducted at the University of Notre Dame at an altitude of 15,000 feet and a Mach of 0.4.[5] A steady startup simulation of 500 iterations was completed to initiate the flow field. An additional unsteady simulation with 2000 time steps was used to ensure the initial transient startup

was convected away from the turret. After the startup was completed, data were gathered for 2000 time steps. The time step was $\Delta t = 5 \times 10^{-6}$ s, so data was collected for a time span of 0.01 seconds, which equals approximately 4.2 "flow-through times" (defined using the turret diameter).

C. Post Processing

i. Beam Analysis

Once the flow has been computed, the analysis of its effect on a laser beam passing through the turret's wake was performed. First, the index of refraction was calculated. The index of refraction, n, is a function of a medium's density as a function of x, y, z, and t, as well as the Gladstone-Dale constant, K_{GD}. Equation 1 gives the index of refraction,

$$n = 1 + K_{GD} \cdot \rho(x, y, z, t). \tag{1}$$

Once the index of refraction is known, the optical path length (OPL) can be calculated. The OPL is a function of the index of refraction and describes the wave front distortion as the beam traverses through a medium. The OPL is found by integrating infinitely thin beams of the light along the propagation path of the beam (whose changing density and thus index of refraction aberrate the wave front, shortening/lengthening the overall distance each ray must travel) over a specified length. Once the OPL is calculated, the spatial average over the whole aperture is computed to obtain $\overline{OPL}$. Figure 9 gives a visual representation of individual light rays travelling through a medium of non-constant density, shortening/lengthening its final path length and giving an overall OPL and $\overline{OPL}$.
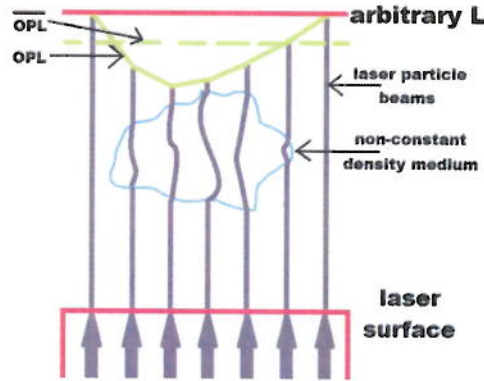

Figure 9. Sketch of beam propagation through a medium of varying density.

Equation 2 shows how OPL is obtained by integrating the index of refraction along the beam path. By substituting n from Eq. 1, Eq. 3 is obtained and makes OPL a function of density and integration length. One assumption made in Eqs. 2 and 3 is that the beam's energy propagates solely in the y direction.

$$OPL(x, z, t) = \int_0^L n(x, y, z, t) dy \tag{2}$$

$$OPL(x, z, t) = L + K_{GD} \int_0^L \rho(x, y, z, t) dy \tag{3}$$

Once OPL and $\overline{OPL}$ are known, optical path difference (OPD) can be calculated. OPD is a measurement of how much the turret's wake distorts the beam's wave front. OPD is found simply by subtracting $\overline{OPL}$ from OPL, seen in Eq. 4. Because OPD changes with time due to the unsteady nature of flow, a root-mean-squared value of OPD, Eq. 5, is used to obtain a value optical engineers can use in combating the effects of changing density on a beam's farfield irradiance.

$$OPD(x, z, t) = OPL(x, z, t) - \overline{OPL(x, z, t)} \tag{4}$$

$$OPD(x, z, t)_{RMS} = \sqrt{\overline{OPD(x, z, t)^2}} \tag{5}$$

The ultimate efficiency of a beam is measured by its end irradiance upon reaching the target. Effective irradiance is measured as a ratio of diffraction-limited irradiance (I) to initial irradiance (I_0). The Strehl ratio is a

5

function of the beam's wavelength as well as $OPD(x,z,t)_{RMS}$, and can be approximated using the Large Aperture Approximation (LAA):

$$Sr = \frac{I}{I_0} = e^{-(\frac{2\pi OPD_{RMS}}{\lambda})^2}.$$

(6)

For a given wavelength λ, the irradiance on target is a direct function of OPD_{RMS}. The chart in Fig. 10 shows theoretical data derived from this premise. In this chart, irradiance decreases exponentially with increasing OPD_{RMS} for any given λ.
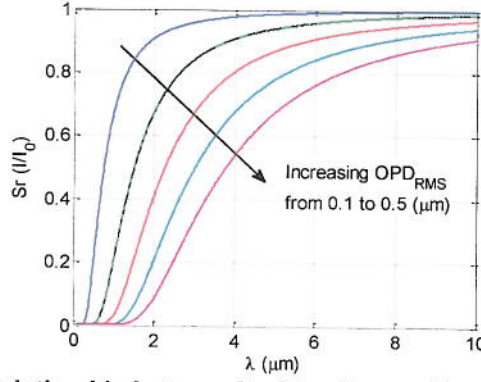

Figure 10. Relationship between Strehl ratio, wavelength, and OPD_{RMS}.[2]

ii. Flow field measurement

For measuring the flow field next to the aperture, there is a ring around the aperture surface of the turret that surrounds the beam with 10,000 nodes. Twenty of these nodes were used to act as pressure ports. These pressure measurements sense the flow field and, in conjunction with actuators (e.g. deformable mirrors), could be used to devise control strategies to mitigate the optical distortions due to the flow near the turret.

III. Results and Discussion

A. Turbulence Model Results

The goal of using the DDES-SST turbulence model was to capture flow structures in the wake relevant to the aero-optics problem. Figure 11 shows an iso-surface of Q colored by density from the simulation using DDES-SST. Figure 12 shows a comparison of the earlier simulations (DDES-SA and no turbulence model) with the DDES-SST result, highlighting the differences in resolved structures.
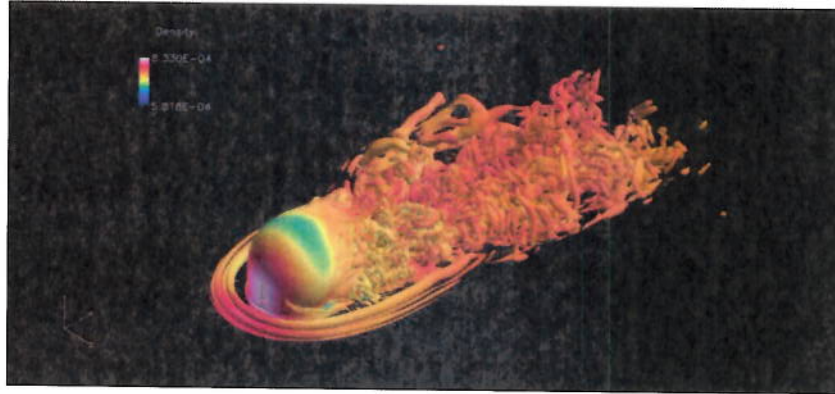

Figure 11. Turret simulation done with DDES-SST turbulence model at Mach 0.4.

The comparison suggests that the DDES-SST model resolved many of the optically relevant flow structures. The shear layer over the aperture still does not show much unsteadiness, but downstream wake vortices that merge with the horn vortices coming off both sides of the turret can be identified. The necklace vortex in the front is reasonably defined and looks like something between the extremely unresolved necklace in the DDES-SA model and the over-resolved necklace in the laminar model.
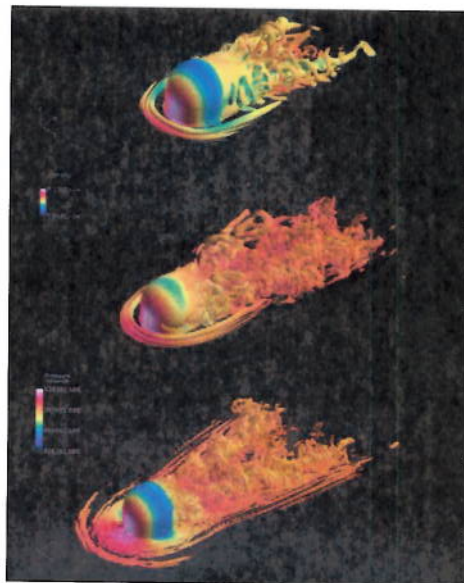

Figure 12. Comparison of DDES-SA turbulence model (top), DDES-SST turbulence model (middle), and laminar model (bottom).

Figure 13 shows the C_P distribution in the center plane over the turret for the DDES-SST simulation as well as previous experimental results (see also Fig.4). Note that the experimental data was obtained using a conformal turret while the computational results were obtained using a turret with a flat aperture and smiles. Within the resolution limits of the experimental data, the simulations capture the separation point reasonably well, although the pressure drop for larger angles is not quite as steep as the experiments indicate. This may in part be due to the limited time history available from the CFD simulations, or geometric differences.
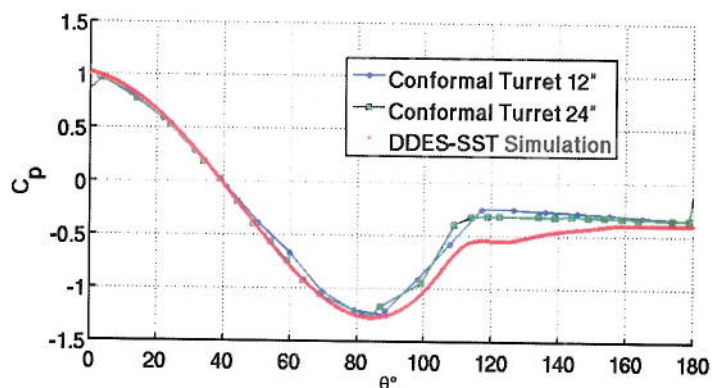

Figure 13. Validation plot using previous data (green and blue lines) with current results (red line).

Figure 14 shows a different isometric view of the flow field that shows the Q iso-surface on the aperture as well as the effect of the smile cutouts. The shear layer over the aperture alters the properties of any beam propagating through it. The shear layer generated by the smile cutouts is negligible for the flow over the aperture in this configuration, but if the elevation angle is 0°, the beam propagates through the shear layer generated by the smile.
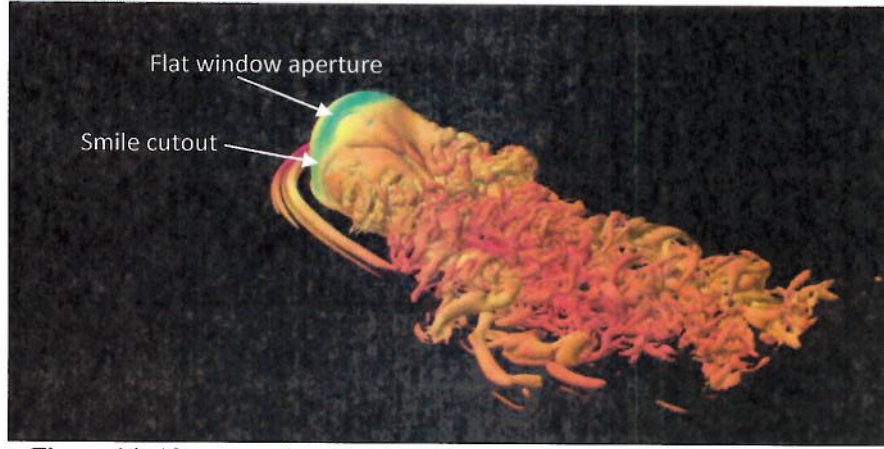
7

Figure 14. Alternate view showing flow around the flat window and smile.

B. Aero Optical Results

The aero optical results, investigating the wave front distortion of a beam emanating from the aperture, were computed using Eqs. 1-6. Figure 15 shows the optical path difference, *OPD*, for this simulation. This figure shows how a normalized cross section, usually shaped like a flat disk, is drastically altered as it propagates through the turret's shear layer.
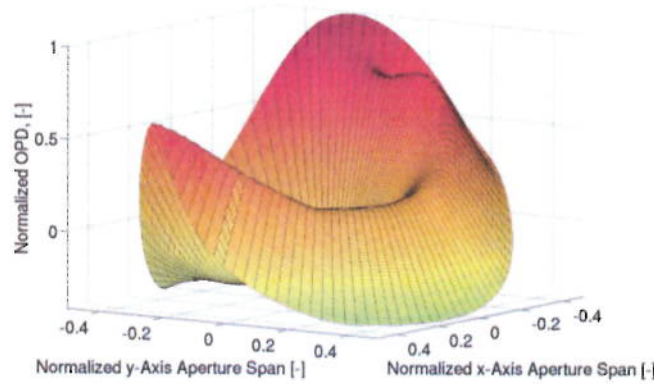

Figure 15. One slice of the laser's *OPD* as it propagates through the turret's shear layer.

One layer of the mesh's beam tap grid has also been overlaid onto the disk seen in Fig. 15 to demonstrate the fineness with which the beam was resolved. The spatial dimensions of the disk have been normalized by the beam diameter, D_b=10 cm. The *OPD* has been normalized by freestream density (ρ_∞=7.71x10^{-4} g/cm^3), square of the Mach number (M=0.4), and turret diameter (D=30.5 cm) as shown in Eq. 7; the resulting unit is μm/m.

$$OPD = OPD_{Norm} \cdot \rho_\infty \cdot M^2 \cdot d \qquad (7)$$

Using these normalized results, static lensing as well as the piston, tip, and tilt distortions (i.e. the distortions described by the first three Zernike polynomials[6]) that affect the beam as it travels through the shear layer can be subtracted. The resulting *OPD* is shown in Fig. 16, which shows that overall *OPD* is significantly reduced.
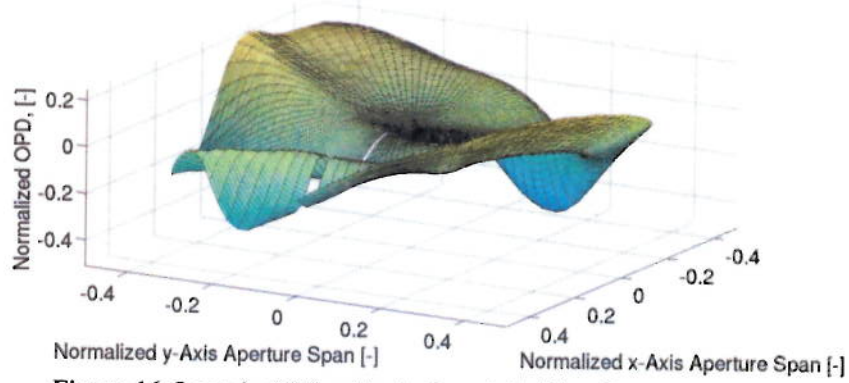
Figure 16. Laser's _OPD_ with static and tip/tilt effects eliminated.

A plot of _OPD_ with successive addition of corrections for static lensing and tip/tilt is shown in Fig. 17. The uncorrected _OPD_ is decreased as corrections are added; interestingly, the effect of tip/tilt removal increases significantly at later times ($\tau = U_\infty \cdot \Delta t / D > 6$), when the uncorrected _OPD_ increases, while the effect of removal of static lensing remains approximately constant.
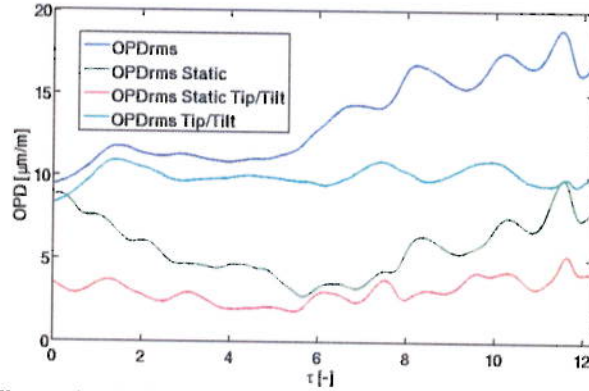

Figure 17. OPD comparison after corrections are added.

The final piece to the aero optics puzzle is effective irradiance in the farfield. Equation 6 is used to compute the Strehl ratio, giving the irradiance that is expected on target. Figure 18 is a plot of irradiance as a function of dimensionless time. As corrections are added and compounded, the Strehl ratio increases, meaning irradiance on target increases, as expected from Fig. 17.
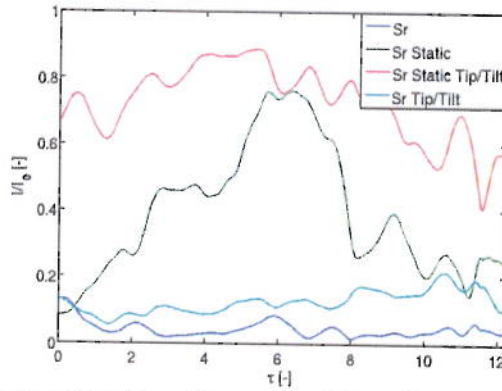

Figure 18. Strehl ratio as a function of normalized time shown with correction effects.

Scrutinizing the data plotted in Figs. 17 and 18, it becomes clear that significant changes in the flow field occurs around $\tau = 6$ and $\tau = 11.5$. At $\tau = 6$, _OPD_ is at its minimum, and the Strehl ratio is at its maximum. The opposite holds

for *OPD* and the Strehl ratio at $\tau=11.5$. In order for the *OPD* to be small and the Strehl ratio to be largest at $\tau=6$, flow structures leading to optical distortions must be absent, i.e. there must be a relatively smooth shear layer over the aperture. Using the same reasoning, at $\tau=11.5$, there must be a large structure disturbing the shear layer, causing *OPD* to be large and Strehl ratio to be low. Inspecting the flow visualization figures at these values of τ, significant differences in the flow field can be observed. Figure 19 shows the flow over the turret at $\tau=6$. The shear layer does not show structures that would affect the aero optics at that point in time. Figure 20, in contrast, at $\tau=11.5$, shows structures on one side of the aperture which significantly affect the aero optics, decreasing the Strehl ratio.
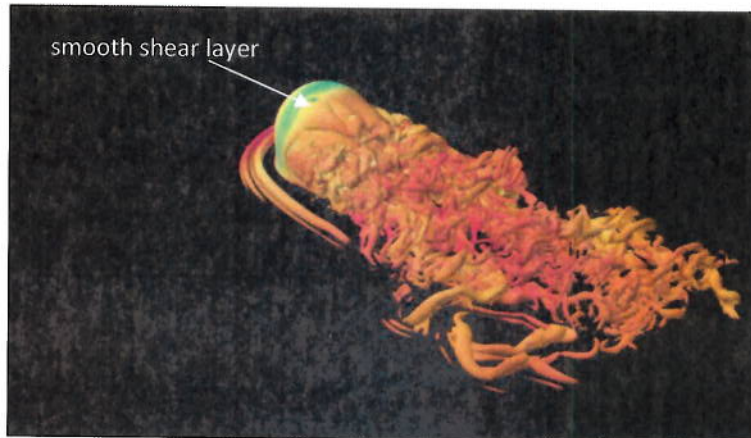

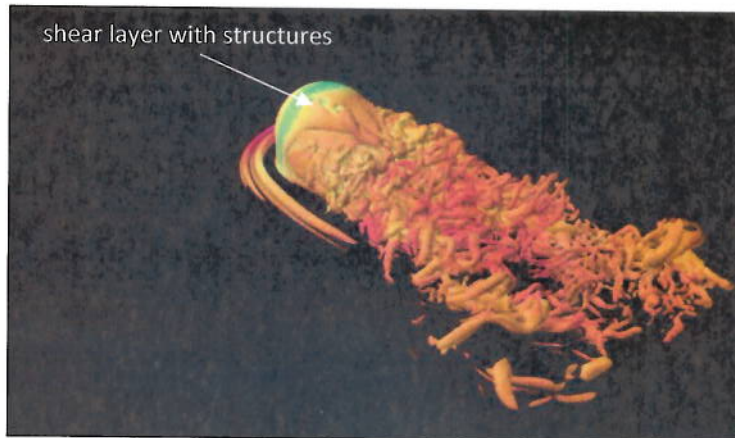**Figure 19. Flow visualization at $\tau=6$ where Strehl ratio is largest.**

Figure 20. Flow visualization at $\tau=11.5$ where Strehl ratio is the smallest.

A comparison of the current simulation results with earlier data (see Fig. 5) is shown in Fig. 21. The results show that the CFD simulation using a turret with a flat aperture and smiles is in good agreement with the experimental data at an azimuth angle of 120°. The geometric modifications of the turret result in significantly different OPD_{norm} values, indicating that the beam propagation is influenced by the smiles, even though the aperture is at an elevation angle of 50°. This in turn leads to the conclusion that there is an unexpectedly strong interaction of the flow over the aperture with the flow around the base of the turret.
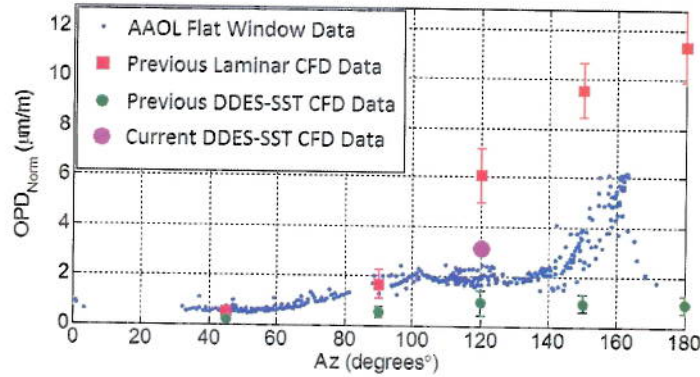
Figure 21. Comparison of current CFD investigation with prior CFD investigations and experiments.

IV. Conclusion

Delayed Detached Eddy simulations with Shear Stress Transport turbulence model were performed to simulate the flow over a generic turret. The flow conditions were chosen to match the flight experiments at an altitude of 15,000ft and a Mach number of M=0.4. The simulations were performed for a flat aperture orientation of 120° azimuth angle and 50° elevation angle. The simulations showed a significant influence of the shear layer, separating at the leading edge of the flat aperture, on the optical performance. Removal of piston and tip/tilt distortions resulted in a marked improvement of optical performance, but unsteady flow structures convecting over the aperture still result in significant optical distortions. Comparing the final OPD_{rms} with the experimental data as well as earlier simulations showed a definite improved match of the current simulations.

References

[1] Zha, G., IM, H., *Delayed Detached Eddy Simulation of a Stall Flow Over NACA0012 Airfoil Using High Order Schemes.* Department of Mechanical and Aerospace Engineering, University of Miami, Coral Gables, FL, 2011.

[2] Seidel, J., Porter, C., Decker, R., "Comparison of Laminar and Turbulent Results." Photograph. *Challenge C4L: Aero-optical distortions in directed energy applications.* PowerPoint. 10 Oct 2012.

[3] Porter, C., Decker, R., Seidel, J., *Modeling Optical Distortions in a Turret Shear Layer for Feedback Flow Control.* USAFA, 2012.

[4] Georgiadis, N. J., Yoder, D. A., Engblom, W.A., *Evaluation of Modified Two-Equation Turbulence Models for Jet Flow Predictions.* NASA Glenn Research Center, Cleveland, OH, 2006.

[5] Porter, C., Gordeyev, S., Zenk, M., Jumper, E., *Flight Measurement of Aero-Optical Distortions from a Flat-Windowed Turret on the Airborne Aero-Optics Laboratory (AAOL).* University of Notre Dame, 2011.

[6] Wang, J. Y., Silva, D. E., *Wave-front interpretation with Zernike polynomials,* Applied Optics, Vol. 19, Issue 9, pp. 1510-1518 (1980)